Experimental study of integer resonance crossing in a nonscaling fixed field alternating gradient accelerator with a Paul ion trap

K. Moriya, K. Fukushima, K. Ito, T. Okano, and H. Okamoto
Graduate School of Advanced Sciences of Matter, Hiroshima University, 1-3-1 Kagamiyama, Higashi-Hiroshima 739-8530, Japan

S. L. Sheehy,* D. J. Kelliher, S. Machida, and C. R. Prior
STFC, Rutherford Appleton Laboratory, Harwell Oxford, Didcot OX11 0QX, United Kingdom
(Received 31 August 2014; published 17 March 2015)

We present an experimental study aimed at exploring integer resonance crossing with a focus on nonscaling fixed field alternating gradient accelerators. The method uses the Simulator of Particle Orbit Dynamics system at Hiroshima University based on a compact ion trap known as a Paul trap. In a setup that mimics the Electron Model for Many Applications nonscaling fixed field alternating gradient accelerator, we have verified the theoretical prediction of the coherent excitation of dipole motion over a wide range of errors and crossing speeds. In addition, the cancellation of amplitude growth dependent on the relative betatron oscillation phase between two consecutive resonances is observed and studied. We also explore nonlinear effects and, in particular, the effects of amplitude-dependent tune shifts and find that these nonlinear effects are a key factor in understanding our experimental results.

DOI: 10.1103/PhysRevSTAB.18.034001 PACS numbers: 29.20.-c, 41.75.-i

I. INTRODUCTION

The nonscaling fixed field alternating gradient (NS-FFAG) accelerator concept was invented in the 1990s [1–4] primarily for the acceleration of muons [5,6]. These accelerators are distinct from the original scaling FFAG invented in the 1950s and 1960s [7], as they employ magnetic fields that do not adhere to the scaling properties of orbit and optics. In particular, the orbits of different momenta are no longer photographic enlargements of each other (i.e., geometric similarity) and focal length no longer scales with the orbit radius (i.e., constant field index k at corresponding orbit points) in the nonscaling version. Both varieties of FFAG have since gained attention for their potential use in other applications including hadron therapy and as high power drivers for neutron production [8–13].

The scaling properties satisfied by the magnetic field $B_y = B_0(r/r_0)^k$ maintain a constant betatron tune, where B_y is the vertical magnetic field, r is the distance from the machine center, B_0 is the vertical magnetic field at $r = r_0$, and k is the field index. By combining a time-independent magnetic field with the stability of alternating gradient focusing, the scaling FFAG achieves a large dynamic aperture and large acceleration range. The orbits in a scaling FFAG are similar from injection to extraction, and the beam moves radially outward during acceleration unless k is chosen to be negative.

By choosing to ignore the scaling restriction, an accelerator lattice designer may introduce attractive properties such as magnet simplicity, design flexibility, and compact orbits. This violation of the scaling properties can be achieved in a number of ways, and as such the NS-FFAG covers a wide spectrum of possible designs [14,15]. The linear nonscaling version of the FFAG was proposed in order to simplify the design to the extent that only linear (quadrupole) fields were required, easing the magnetic construction. This is the type of accelerator recently constructed and commissioned in the United Kingdom at Daresbury Laboratory, called EMMA, the Electron Model for Many Applications [16,17].

This violation of the scaling properties naturally leads to consequences in the beam dynamics of the NS-FFAG. One consequence is flexibility in the time of flight variation with momentum, allowing a novel rapid acceleration scheme called "serpentine acceleration" in some cases [18]. A further feature of the linear NS-FFAG is that the radial orbit excursion can be reduced compared to its scaling counterpart. However, the most relevant beam dynamics feature for this work is that the scaling violation leads to a variation of betatron tune with momentum, or a large uncorrected chromaticity. This leads to resonance-crossing phenomena during acceleration.

While other accelerators may routinely or experimentally cross low-order resonances [19], linear NS-FFAGs including EMMA are unique in routinely crossing multiple

*Corresponding author.
Suzie.Sheehy@stfc.ac.uk

first-order integer resonances, in some cases more than ten times per acceleration cycle. Naturally, one should expect negative consequences of such a design feature. It is, however, widely held that, in the case of fast resonance crossing, betatron amplitudes will not grow significantly and the beam will not deteriorate. Successful fast acceleration in EMMA using the serpentine channel has indeed been demonstrated [17]. However, the parameter space that EMMA may explore experimentally is limited due to the present acceleration scheme (serpentine acceleration) and the fixed rf of the installed cavities [20].

Many potential applications of NS-FFAGs rely on the acceleration of protons or other hadrons. In such designs, fast acceleration in very few turns is not always feasible, and slower resonance crossing may deteriorate the beam quality or necessitate extremely small alignment tolerances. The two fundamental parameters driving such resonances are the level of dipole imperfections and the rate of change of the tune, or resonance-crossing rate [21,22]. A more fundamental understanding of integer resonance crossing over a wide range of operational parameters is required to explore the application of NS-FFAG accelerators with slower acceleration rates. Theoretical predictions of the coherent excitation of dipole motion exist but are difficult to evaluate experimentally. Investigating this phenomenon in a real accelerator is problematic over the necessary parameter range, and, even if it were possible, such a study would be extremely time consuming. Likewise, simulations are a very useful tool but cannot be substituted for experimental verification. Establishing such an understanding experimentally is the purpose of this work.

In order to make a systematic experimental study of resonance crossing over a wide range of parameters, we employ a tabletop experimental tool Simulator of Particle Orbit Dynamics (S-POD) developed at Hiroshima University. S-POD is a compact non-neutral plasma trap facility based on the idea first proposed in Ref. [23] for fundamental beam physics purposes. This unique apparatus provides, in the laboratory frame, a many-body Coulomb system physically equivalent to a charged particle beam in an alternating gradient focusing channel, thus enabling the exploration of important beam dynamics issues without relying on large scale accelerators [24–29]. It should be noted that one limitation of such a trap is the absence of any momentum dispersion effects. However, these are not expected to play a large or dominant role in the present studies.

While the application of two different types of plasma trap has been discussed in Ref. [23], we here choose the so-called *linear Paul trap* (LPT) where a rf quadrupole field is used for particle confinement [30]. Figure 1 shows an overall view of the S-POD employed for the present resonance-crossing experiment [31]. The multisectioned LPT of about 20 cm in length is operated at 1 MHz and located in a vacuum chamber. A similar LPT-based apparatus has been constructed and employed for beam physics at Princeton Plasma Physics Laboratory [32–35]. Since a detailed explanation of the operation of S-POD has been given in past publications [23–28], we do not repeat it here.

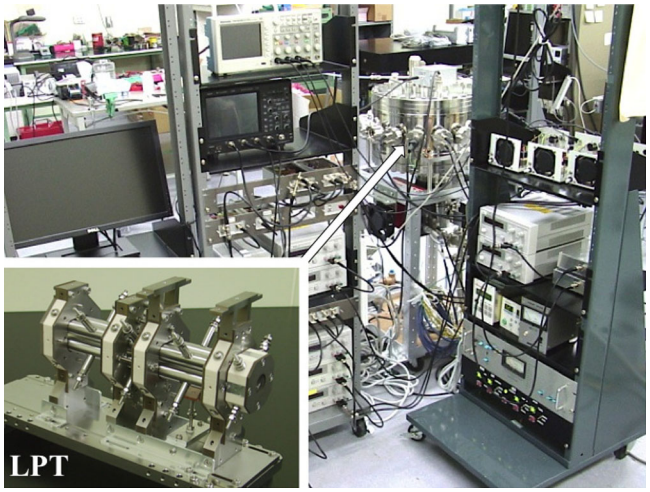

FIG. 1. An overall view of the S-POD system employed for the present resonance-crossing experiment. A compact LPT (lower left corner) has been installed in the chamber inside which the vacuum pressure is kept lower than 10^{-7} Pa. The main S-POD components, including an electron gun for neutral gas ionization, data-taking system, and ac and dc power supplies, are controlled by a personal computer, so that all the necessary experimental procedures are executed automatically.

In our previous work [27], extensive experimental and numerical results were reported on linear (quadrupole-driven) and low-order nonlinear (sextupole- and octupole-driven) resonance crossing. We now pay particular attention to integer resonance crossing. Such resonances do not generally occur in a regular LPT because of the symmetric excitation of the four LPT electrodes, which eliminates a periodic dipole component in the plasma confinement field. Here we intentionally introduce an rf dipole field to generate stop bands of integer resonances [28,35]. Considering the typical low-intensity conditions of EMMA operation, a relatively small number of ions are confined in the LPT, to ensure that collective space charge effects remain negligible. As in past experiments, we choose $^{40}Ar^{+}$ among possible candidates of ion species. In principle, it does not matter which ion species is used, because the ion mass and charge state are simply scaling parameters in S-POD experiments [23,24].

In Sec. II, we start by describing the EMMA parameters. This section is also devoted to justifying the applicability of S-POD to the present purpose. After explaining the correspondence between plasma parameters in S-POD and beam parameters in the NS-FFAG, we show experimentally that resonant instabilities can be excited at integer bare tunes with the addition of a rf dipole field. Results of resonance-crossing experiments are then given in Sec. III. These results first verify the theory of integer resonance

crossing by making the beam cross a single resonance. We then show the more realistic situation in a linear NS-FFAG, that is, the case of multiple resonance crossing. In Sec. IV, we discuss the interpretation of the experimental results and the effects of nonlinearities. Concluding remarks are addressed in Sec. V.

II. EMMA AND ITS MODEL S-POD

A. Linear NS-FFAG EMMA

EMMA is a linear NS-FFAG for electrons, the main parameters of which are given in Table I. The design consists of 42 doublets of quadrupoles in which the dipole component is achieved by simply sending the beam through the quadrupoles off axis. The magnets are mounted on precise slider mechanisms in order to vary the bending and focusing field components independently. In general, the predominant driving forces for integer resonances in a linear NS-FFAG are alignment errors of the quadrupole magnets that cause dipole field errors and errors in the dipole magnetic field itself if such a field is present [36].

The transverse closed orbit distortion (COD) in a circular accelerator due to a dipole error field $\Delta B/B$ is well known and obeys the differential equation

$$\frac{d^2x_{\mathrm{COD}}}{ds^2} + K_x(s)x_{\mathrm{COD}} = -\frac{\Delta B}{B\rho}, \tag{1}$$

where ρ is the local curvature of the design beam orbit, s is the path length, and K_x is the magnetic quadrupole focusing function determined by the machine lattice. When the average radius of the machine is R, application of the smooth approximation to Eq. (1) yields

$$\frac{d^2x_{\mathrm{COD}}}{d\theta^2} + \nu_0^2 x_{\mathrm{COD}} = -R^2\frac{\Delta B}{B\rho}, \tag{2}$$

where ν_0 is the bare tune and the angle $d\theta(=ds/R)$ increases by 2π every single turn. The dipole error is periodic and can thus be expanded into a Fourier series as $\Delta B/B\rho = \sum_j b_j \cos(j\theta + \phi_j)$, where b_n and ϕ_n are constant parameters. The solution to Eq. (2) diverges when ν_0 is an integer (integer resonance).

TABLE I. Main parameters of the EMMA NS-FFAG.

Energy range	10–20 MeV
Cell type	FD doublet
Number of cells	42
rf	1.301 GHz
rf voltage	0.2–2.0 MV with 19 cavities
Integrated quadrupole gradient	0.402/−0.367 T (QF/QD)
Cell length	394.481 mm
Ring circumference	16.568 m

B. Determination of the rf dipole amplitude

As mentioned above, the LPT is, in principle, free from integer resonances. A dipole driving force can, however, be provided by applying additional rf voltages to one or two of the four quadrupole electrodes [28,35]. We apply either pulsed or sinusoidal perturbing voltages of opposite signs to two horizontal electrodes, as illustrated in Fig. 2. By neglecting nonlinearity of the transverse rf focusing fields and the space charge potential, the equation of the transverse ion motion in a LPT with a dipole driving field can be written as

$$\frac{d^2x}{d\tau^2} + K_{\mathrm{rf}}(\tau)x = -\frac{q\xi}{mc^2r_0}V_D(\tau), \tag{3}$$

where m and q are the mass and charge state of confined ions, respectively, r_0 is the minimum distance to the electrode surface from the trap axis (in other words, the radius of the LPT aperture $r_0 = 5$ mm), $\tau = ct$ with c the speed of light, K_{rf} is the rf quadrupole focusing function, ξ is a constant factor depending on the geometry of the quadrupole electrodes ($\xi = 0.795$ in this case), and V_D is the dipole perturbation voltage indicated in Fig. 2. When the amplitude of the rf quadrupole voltages applied to the four electrode rods is V_Q, K_{rf} is equal to $K_{\mathrm{rf}}(\tau) = 2qV_Q(\tau)/mc^2r_0^2$.

We now consider a NS-FFAG composed of P identical doublet focusing cells. In the EMMA case, $P = 42$. A single turn around the machine then corresponds to P sinusoidal periods in the function K_{rf} (see Fig. 3). The time dependence of K_{rf} in Eq. (3) is smoothed to give

$$\frac{d^2x}{d\theta_P^2} + \nu_0^2 x = -\left(\frac{P\lambda}{2\pi}\right)^2\frac{q}{mc^2r_0}V_D(\theta_P), \tag{4}$$

where λ is the wavelength of single rf focusing period in the LPT and the angle $\theta_P(=2\pi\tau/P\lambda)$ increases by 2π every turn. In general, the dipole perturbation V_D is periodic with a periodicity of 2π and can be expressed, similarly to $\Delta B/B$, as $V_D = \sum_j w_j \cos(j\theta_P + \phi_j)$, where w_j and ϕ_j are

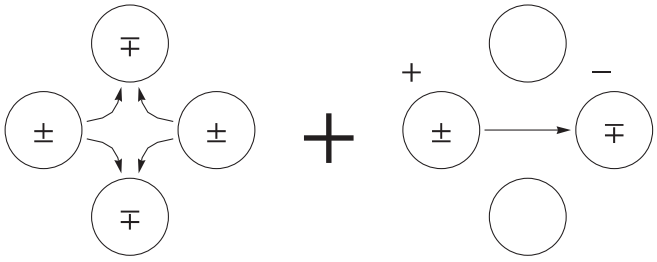

FIG. 2. rf voltages applied to the quadrupole electrodes of the LPT. In addition to the regular rf power of quadrupole symmetry (left), we simultaneously introduce the dipole rf perturbation (right) to excite integer resonance.

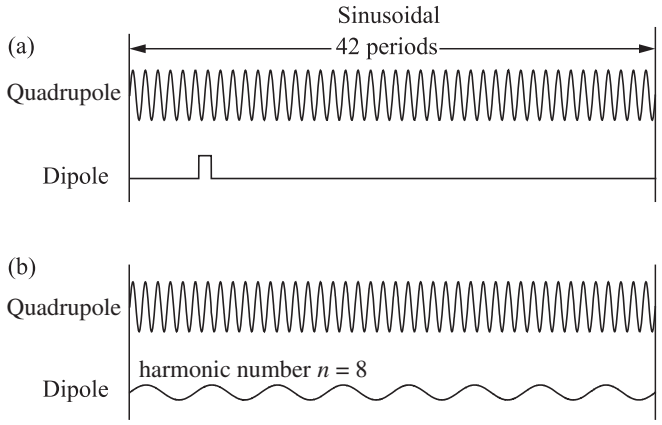

FIG. 3. Typical waveforms of the driving rf voltages applied to the LPT electrodes. The doublet focusing is approximated by a sinusoidal waveform oscillating at 1 MHz. As for the dipole perturbation, two different rf waveforms are considered, namely, (a) a piecewise constant voltage emulating the local dipole field error such as a leakage field from the septum magnet in EMMA and (b) a sinusoidally varying voltage corresponding to a single Fourier harmonic of the pulse voltage in (a).

constants. The on-resonance solution to Eq. (4), i.e., the diverging orbit under the condition $\nu_0 = n$, is given by

$$x = x_0 \cos(n\theta_P + \alpha) - \frac{1}{2}\left(\frac{P\lambda}{2\pi}\right)^2 \frac{q}{mc^2 r_0}\frac{w_n \theta_P}{n}\sin(n\theta_P + \phi_n) - \left(\frac{P\lambda}{2\pi}\right)^2 \frac{q}{mc^2 r_0}\sum_{j\neq n}\frac{w_j}{n^2 - j^2}\cos(j\theta_P + \phi_j), \quad (5)$$

where x_0 and α are constant. Comparing the driving term in Eq. (4) with that in Eq. (2), we find that the physical orbit distortions in these systems are similar when

$$V_D \approx \frac{mc^2 r_0}{q\xi}\left(\frac{2\pi R}{P\lambda}\right)^2 \frac{\Delta B}{B\rho}. \quad (6)$$

This formula allows us to make a quick estimate of the dipole rf voltage V_D equivalent to the strength of a certain error field $\Delta B/B$.

C. Excitation of resonances

To verify that we can excite and control integer resonance stop bands in S-POD, two different rf waveforms as shown in Fig. 3 were employed for V_D. In the upper case, the dipole perturbation is piecewise constant within a narrow range, which emulates a once-per-turn dipole field error like the local septum leakage field in EMMA. Only one of many Fourier harmonics (the eighth harmonic in this example, namely, $w_n = 0$ except when $n = 8$) is extracted from V_D in the lower case. For the primary quadrupole focusing potential, we use a sinusoidal waveform for the sake of simplicity to approximate the doublet lattice. Since EMMA is composed of 42 identical doublet cells, 42 consecutive sinusoidal rf periods correspond to a single turn around the ring. It has been demonstrated numerically and experimentally that sinusoidal focusing has a resonance feature analogous to that of discrete doublet focusing [29]. Note also that symmetric transverse focusing has been assumed throughout this work. Thus, the horizontal and vertical tunes are always equal. We employ this simplest experimental case in order to study the fundamental beam dynamics effects of integer resonance crossing.

First of all, we experimentally determine the stop-band distribution without the dipole perturbation. About 10 000 $^{40}Ar^+$ ions are initially trapped in the LPT and stored for 10 ms at a certain fixed value of bare tune ν_0. The number of ions surviving after the 10 ms storage is measured with a microchannel plate (MCP) positioned at the one end of the LPT. The same experimental procedure was repeated many times, changing ν_0 in small steps over a wide range. Figure 4(a) shows the stop-band distribution measured in S-POD without the dipole perturbation. We observe three clear stop bands near $\nu_0 \approx 42/6$, $\nu_0 \approx 42/4$, and $\nu_0 \approx 42/3$, corresponding, respectively, to sixth-, fourth-, and third-order resonances. The primary source of these resonances is weak nonlinear focusing components induced mostly by the misalignment of the quadrupole rods. We confirm in Fig. 4(b) that the application of the piecewise constant dipole perturbation in Fig. 3(a) generates stop bands at every integer tune, in addition to the three original stop bands in Fig. 4(a). In this example, the height and width of the dipole pulse are fixed at 1 V and 1 μs, respectively. The use of the sinusoidal perturbation in Fig. 3(b) eliminates all integer stop bands except for the one located at $\nu_0 = 8$, as experimentally verified in Fig. 4(c). We can readily excite an arbitrary number of stop bands at arbitrary integer tunes by applying several sinusoidal perturbation waves of different harmonics simultaneously.

D. Ion losses on resonance

Before proceeding to resonance-crossing experiments, we first check how quickly the amplitude of the transverse plasma oscillation grows on resonance. We can estimate the growth rate of the transverse amplitude by measuring the number of ions after a certain period of time with the MCP detector. An ion plasma is initially produced through the electron bombardment process. After an ionization process that lasts for many rf periods (typically 200 ms), we wait for another 50 ms so that the plasma approaches a steady state. We thus assume that the initial ion distribution is approximately Gaussian.

As an example of on-resonance loss, let us take a look at the ion loss behavior on the integer resonance driven by the eighth harmonic, namely, the time evolution of ion losses when the LPT operating point is in the middle of the stop band at $\nu_0 = 8$ in Fig. 4(c). To ensure there is no systematic

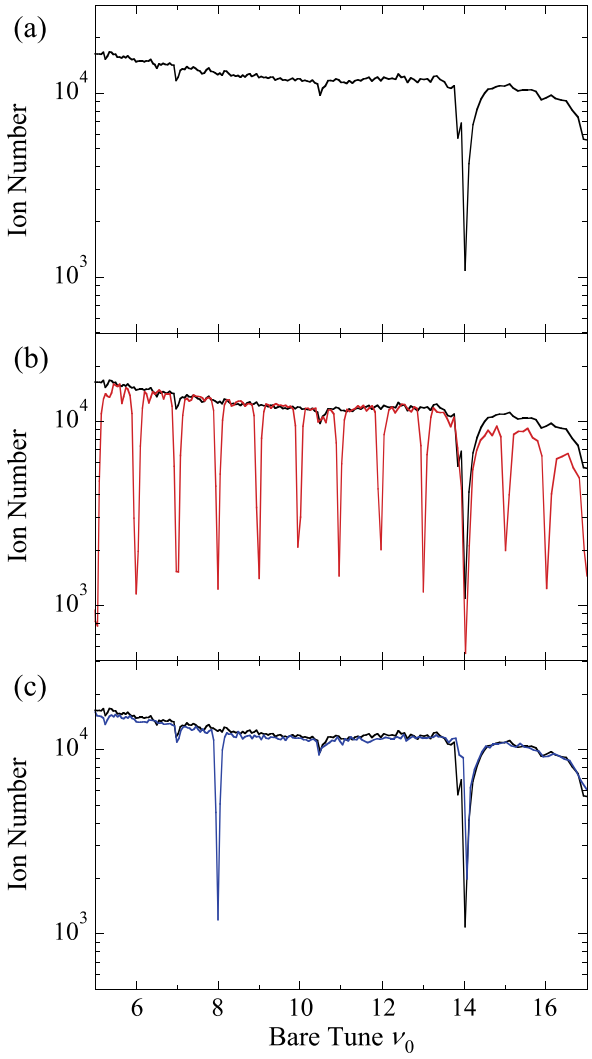

FIG. 4. Resonance stop bands identified by the S-POD system. Starting with roughly 10^4 ions in the LPT, we measured the final ion number after 10 ms at various fixed tunes. There are 140 data points of independent measurements in the tune range $5 \leq \nu_0 \leq 17$. (a) Stop-band distribution with no dipole perturbation, (b) stop-band distribution with a piecewise constant dipole perturbation whose pulse height and width are 1 V and 1 μs, respectively, and (c) stop-band distribution with a sinusoidal dipole perturbation as shown in Fig. 3(b). For reference, the data of the case (a) is replotted with a black solid line in the middle and lower pictures.

error in setting the primary focusing frequency, an initial tune scan is performed. The selected tune is that which produces maximum ion losses corresponding to the center of the stop band. The results of S-POD measurements are given in Fig. 5 together with the corresponding WARP simulation data plotted by a solid line [37]. (Three independent approaches were used to cross-check numerical results and are discussed in more detail in Appendix A.) The abscissa is not the simple time variable but has been scaled by the amplitude w_n of the eighth dipole harmonic, because the diverging term in Eq. (5) is proportional to

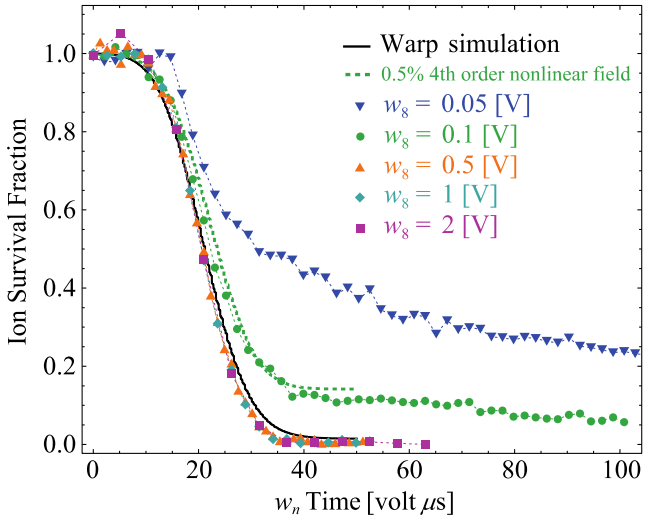

FIG. 5. Time evolution of ion losses when the LPT operating point is fixed exactly on the integer resonance at $\nu_0 = 8$ in Fig. 4(c). Five different sinusoidal amplitudes are considered to change the resonance strength. The solid curve represents the corresponding WARP simulation result in which perfectly aligned quadrupole rods have been assumed, and the dashed curve where nonlinearities have been introduced. The initial plasma temperature is set at 0.5 eV.

$w_n\theta_P$. Various different values of w_n are considered corresponding to different strengths of a dipole error source in EMMA.

In Fig. 5, we have chosen w_n to be sufficiently low to avoid instant ion losses. We find that the loss behavior is always similar [as predicted by Eq. (5)] and agrees well with the WARP simulation unless the dipole perturbation is very small. The WARP simulations were done with a much wider range of choices of w_n, but no substantial difference was found. By contrast, the experimental results with very low w_n (less than 0.1 V) are clearly different from the others. The deviation from the ideal numerical result becomes larger as w_n is lowered. This could be caused by nonlinearity of the focusing in the trap, which introduces an amplitude-dependent tune shift. Without the perturbation, there is no beam loss on the time scale of a few milliseconds as shown in Fig. 4(a). More detail on this effect is discussed in Sec. IV.

E. Amplitude growth off resonance

The typical time evolution of an on-resonance transverse plasma profile observed on a phosphor screen is shown in Fig. 6, where $w_8 = 0.1$ V. As the image is axially integrated over many rf periods during plasma extraction, it is expected that the transverse closed orbit distortion will be observed as an increase in transverse size even when the tune is not at an integer. To verify this, first the dipole perturbation is ramped up slowly over a period of 0.1 ms in order to minimize coherent oscillations around the distorted

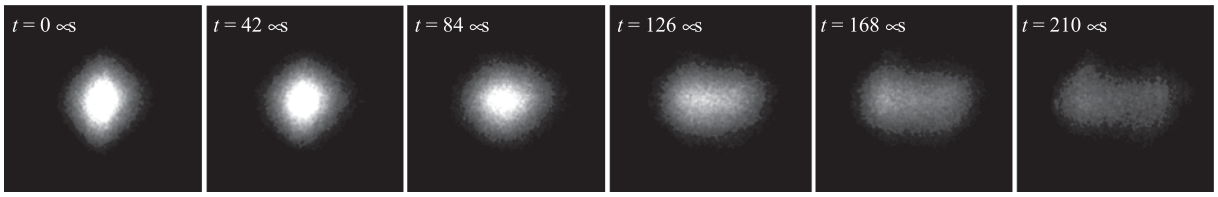

FIG. 6. Time evolution of a transverse plasma profile on the phosphor screen measured with a CCD camera. The bare tune of the LPT and the perturbation amplitude are set, respectively, at $\nu_0 = 8$ and $w_8 = 0.1$ V. The initial number of Ar^+ ions is increased to 3.2×10^5 in order to enhance the phosphor images. Note that each image does not reflect the plasma profile at a specific moment but is an axially integrated signal over many rf periods. The two electrode rods with the dipole perturbation are located in the horizontal direction (see Fig. 2).

closed orbit. We then experimentally observe the change in the integrated phosphor screen image after a given accumulation time while the tune is set to a fixed value, some distance from the integer.

As the perturbation strength is increased, we see a corresponding increase in the closed orbit distortion as a widening of the horizontal FWHM of the integrated distribution. Further from the resonance, no widening is observed.

This method is repeated for a range of perturbation voltages for a set tune value of $\nu_0 = 8.1$, and the results are shown in Fig. 7. Each experimental data point is the mean of 40 repeated experiments to ensure the results are not affected by any statistical fluctuations in the focusing waveform voltage or extraction timing.

The fact that the bunch oscillates during extraction means the theoretical comparison to the horizontal FWHM is not trivially the same as the COD amplitude. To establish the relationship between theoretical FWHM and COD amplitude, we start by assuming a Gaussian bunch whose width is calculated from the zero perturbation experimental case. This Gaussian is then integrated numerically with the mean following a time-dependent COD trajectory for many oscillation periods. The resulting translation from perturbation strength to amplitude and then to FWHM using this method is shown as the "lossless theory" curve in Fig. 7.

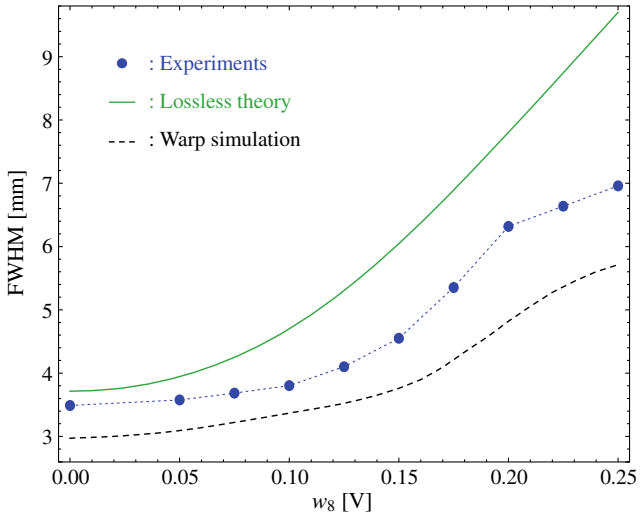

FIG. 7. Measured growth in horizontal FWHM as a function of perturbation strength w_8 calculated from integrated phosphor screen images. The tune is set to $\nu_0 = 8.1$, and the dipole perturbation is excited at the eighth harmonic.

We note that the experimental FWHM is slightly smaller than that predicted by theory, which may be caused by the aperture of the trap removing large-amplitude particles in the distribution tails. A 2D simulation with WARP including particle loss on the aperture produces a qualitatively similar result to the experimental data, although the simulated FWHM is lower for each point due to the initial plasma temperature assumption of 0.5 eV, which produces a slightly different FWHM for the initial distribution compared to the zero perturbation experimental case.

Coupling effects between the horizontal and vertical planes may also be playing a role, and preliminary data suggest that for high perturbation strength there may be a small increase in vertical amplitude also. While this effect does not impact significantly on the results contained herein, a detailed study of coupling effects is a topic of ongoing work.

III. INTEGER-RESONANCE-CROSSING EXPERIMENT

Having established the excitation of integer resonance stop bands and observed the resulting amplitude growth, we now proceed to integer-resonance-crossing experiments. In S-POD, the operating point can be ramped at a given speed from an initial tune to another final tune by ramping the rf quadrupole amplitude V_Q from one value to another. Unlike in previous sections, this tune-ramping process is dynamic rather than a series of static tune experiments. While either direction of tune variation, upward or downward, is feasible in S-POD, here we consider only the downward resonance crossing that occurs during acceleration in linear NS-FFAGs. Following Ref. [27], we define the resonance-crossing speed u as the ratio of δ (the width of tune variation per single focusing cell) to n_{rf} (number of rf periods for the bare tune to go across the width δ) in units of cell tune per cell. For

example, a single ring of the proton therapy design in [11] with 1000-turn acceleration has $u \approx 4 \times 10^{-6}$. In the case considered here, we assume 10-turn extraction of an electron beam from EMMA, where u is roughly 5×10^{-4} if the tune per cell decreases by 0.2 during acceleration. First we verify the theory of integer resonance crossing by making the plasma cross a single resonance. We then present the results of the more realistic multiple resonance-crossing case in a linear nonscaling FFAG.

A. Single resonance crossing

We first explore what happens when the LPT operating point crosses a single integer resonance stop band. In order to see the effect from a single stop band, the single harmonic perturbation case (c) in Fig. 4 was adopted instead of the general case (b). The integer stop band at $\nu_0 = 8$ is almost completely isolated in this case, except for a weak nonlinear resonance at $\nu_0 = 42/6$. The operating bare tune ν_0 is varied from the initial value of 9.5 down to 7.5 at various speeds. The rate of Ar^+ ions surviving after resonance crossing is plotted as a function of the crossing speed u in Fig. 8. Several different rf amplitudes are chosen for the dipole perturbation. Filled symbols are experimental results, while open symbols come from numerical simulations by the WARP code [37]. The numerical data are in good agreement with the experimental observation. The slightly higher results from the simulation arise due to the sensitivity of ion loss to assumptions about the exact initial ion distribution. A similar systematic experiment of single resonance crossing was done with the twelfth harmonic w_{12} to excite another isolated stop band to cross-check this result. Essentially the same results as shown in Fig. 8 were obtained for crossing the stop band at $\nu_0 = 12$.

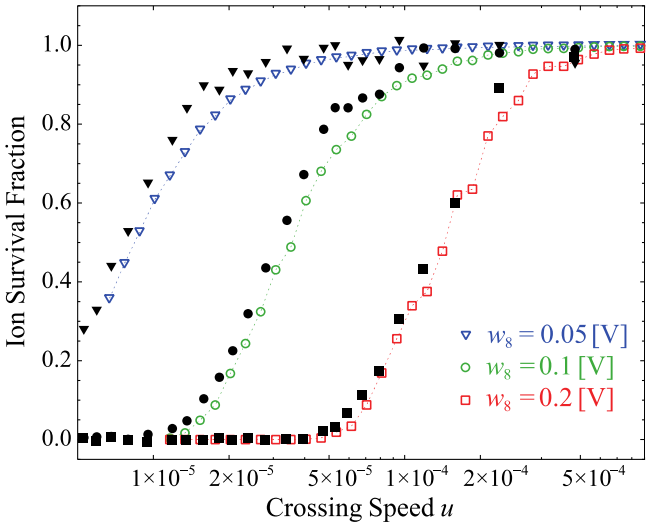

FIG. 8. Fraction of ions remaining after integer resonance crossing. Fractional ion losses obtained with various dipole perturbation strengths are plotted as a function of crossing speed u. The bare tune ν_0 is reduced from 9.5 to 7.5. Filled and open symbols show, respectively, experimental data and WARP simulation results in which the initial ion distribution is Gaussian with a temperature of 0.5 eV.

Guignard derived a formula to estimate coherent amplitude growth after a single integer resonance crossing [38]:

$$\Delta\sqrt{\varepsilon} = \frac{\pi}{\sqrt{Q_\tau}}\frac{2R}{B\rho}\left|\frac{1}{2\pi}\int_0^{2\pi}\sqrt{\beta}\Delta B \exp(in\theta)d\theta\right|, \qquad (7)$$

where ε is the amplitude of the coherent excitation of the dipole motion, Q_τ is the rate of change of tune per turn, and β is the betatron amplitude parameter. Appendix B discusses the nonsmooth and smooth approximations to estimate coherent amplitude growth. Using the relation (6) together with the Fourier coefficients w_n and b_n, we eventually obtain the following approximate dipole oscillation amplitude in terms of S-POD:

$$\Delta A_n = g_n^{\mathrm{G}}\frac{w_n}{\sqrt{u}}, \qquad (8)$$

where $g_n^{\mathrm{G}} = \frac{q\lambda}{2\pi mc^2 r_0}\max(\sqrt{\beta_{\mathrm{rf}}})\left|\int_0^{2\pi}\sqrt{\beta_{\mathrm{rf}}}\sin(n\theta_P)\exp\times(in\theta_P)d\theta_P\right|$ with β_{rf} defined by $\beta_{\mathrm{rf}} = (P\lambda/2\pi R)\beta$. Figure 9 shows how ΔA_8 depends on the crossing speed. The solid curve is based on Guignard's formula when the maximum dipole oscillation amplitude reaches the LPT aperture of 5 mm. Results of S-POD measurements are plotted with black dots. Here, the experimental critical perturbation voltage corresponding to the centroid of plasma oscillations reaching the aperture limit of 5 mm in S-POD is estimated from the experimental ion loss at a particular crossing speed as follows: As the plasma centroid starts to oscillate on an integer resonance, the plasma is

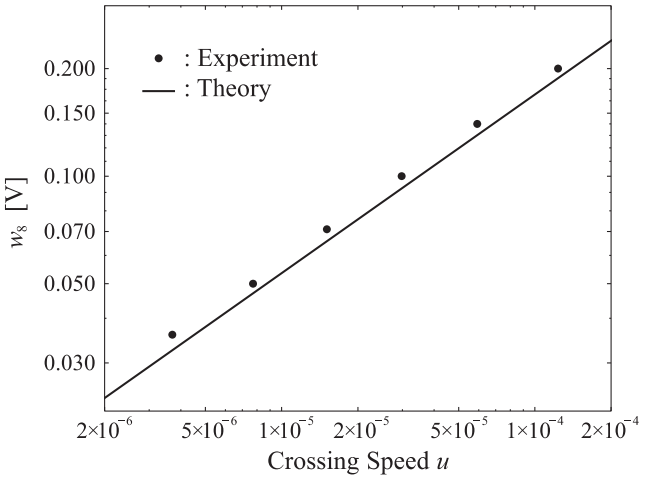

FIG. 9. Crossing-speed dependence of the critical perturbation voltage at which the maximum transverse shift of the plasma centroid reaches 5 mm (the LPT aperture) after single resonance crossing at $\nu_0 = 8$. The solid curve is a theoretical estimate with the nonsmooth formula. Black dots are experimental data from S-POD.

scraped by the two horizontal electrodes. Since the oscillation frequencies of individual ions are identical to that of the plasma centroid oscillation about the trap axis, the ions remain in synchronous rotation about the trap axis. Therefore, roughly half of the ions confined in the LPT should hit the electrode surface when the horizontal shift of the original plasma approaches the aperture size (5 mm in radius). The black dots in Fig. 9 represent the measured perturbation voltage V_D at which 50% of initial ions are lost after crossing the stop band at $\nu_0 = 8$. We confirm that the theoretical estimate from Eq. (8) agrees fairly well with S-POD data.

B. Additional effects of multiple resonance crossing

In practice, the operating point of a NS-FFAG crosses not one but more likely several integer stop bands. It is thus important to ask whether any new features appear when a few stop bands are crossed consecutively. Previous simulation studies have shown interesting beam behavior expected in multiple resonance crossing [39] in which the phase of errors may not add and in some instances may even cancel. To investigate this issue systematically, we now introduce the ninth dipole harmonic in addition to the eighth considered in the last section. The amplitudes of both harmonics are always set equal here for simplicity.

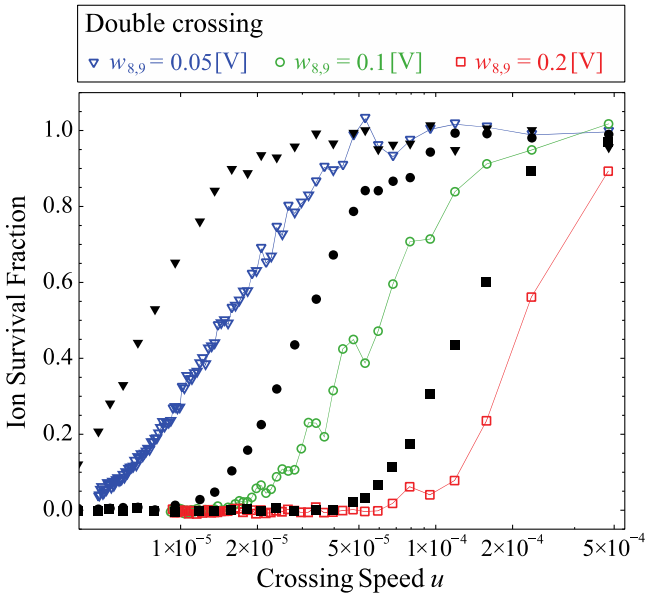

FIG. 10. Results of double resonance-crossing experiments. Two integer resonances at $\nu_0 = 8$ and 9 are consecutively crossed at various speed u. The amplitudes of the eighth and ninth dipole driving harmonics are set equal to 0.05 (triangle), 0.1 (circle), and 0.2 V (square). The rf phases of both sinusoidal waves are fixed at 0° at the beginning. The tune variation range is the same as that considered in the previous single resonance-crossing experiment in Fig. 8; namely, the initial tune is 9.5 eventually reduced to 7.5. For reference, the corresponding experimental data of *single* resonance crossing are plotted with black symbols.

The operating tune is swept from 9.5 to 7.5 traversing the two stop bands. Three independent series of S-POD experiments were carried out with three different strengths of the dipole perturbation and are summarized in Fig. 10. The ion loss rate has been clearly enhanced compared to the case of single resonance crossing.

We recognize in Fig. 10 that the ion loss curve is not very smooth but has small oscillatory structure at particular crossing speeds. The mechanism of this phenomenon can be understood by considering the effect of the second integer tune crossing at $\nu_0 = 9$ on the transverse plasma oscillation excited by the first integer tune crossing at $\nu_0 = 8$. After the first crossing, the whole plasma starts to execute a centroid coherent oscillation whose tune is gradually changing from 9 toward 8. The change in phase of the oscillations during the shift of operating point depends on the crossing speed u. The effect of a second crossing on the dipole motion depends on the oscillation phase. This phase dependence has been studied in more detail in Sec. IV B and also with simulations discussed in Appendix C.

IV. DISCUSSION

A. On-resonance ion loss plateau

In Sec. II D, when the tune of the trap is set to an integer resonance and a finite perturbation is applied, we expect the amplitude of the plasma oscillation to grow without bound. In fact, Fig. 5 shows this does not happen when the dipole perturbation strength is sufficiently low. Instead, the amplitude initially increases and then reaches a plateau.

We consider two possible explanations for this. The first is that an amplitude-dependent tune shift results in the tune moving away from the resonance. This may be caused by electrode imperfections or misalignments exciting higher-order multipoles, where an octupole term would give rise to detuning with amplitude. The second very simple explanation is that a systematic operating error has caused the tune to be set slightly away from the resonance and the plateau we observe corresponds to the resulting finite COD.

In the first scenario, we can assume a linear detuning with action

$$\nu_x = \nu_{x0} + \mu_D I_x, \tag{9}$$

where μ_D is the detuning parameter, ν_{x0} is the tune at zero action, I_x is the action, and the altered tune is ν_x. It has been shown in this case that the centroid amplitude $x_C \propto (w_n/\mu_D)^{1/3}$ [40]. On the other hand, in the case of an operating tune error, the COD grows linearly with perturbation voltage: $x_C \propto w_n$.

The two hypotheses can be tested by measuring how x_C varies with w_n experimentally. We cannot measure the centroid amplitude directly, so we have to infer it from the ion loss data, assuming the plasma can be represented by a transversely shifted 1D Gaussian. Since the tune is on an

integer resonance or close to it, the plasma can be assumed to oscillate synchronously around the trap axis. In that case, the fraction of ions ζ that remain within the aperture is given by the complementary error function:

$$\zeta = 1 - 0.5\mathrm{erfc}\left(\frac{r_0 - x_C}{\sqrt{2}\sigma_x}\right), \tag{10}$$

where the size of the plasma distribution σ_x is obtained from CCD measurements. Rearranging in terms of ζ, one obtains

$$x_C = r_0 - \sqrt{2}\sigma_x \mathrm{erfc}^{-1}(2 - 2\zeta). \tag{11}$$

Using this equation, the evolution of the centroid amplitude can be obtained from the ion survival data in the plateau phase. An extended set of ion loss data and the resulting fit are shown in Fig. 11 (lower) along with a power law fit to the function $x_c = aw_n^b$, where a and b are fitting parameters. The highest three perturbation voltages were excluded from the fit, since the low number of ions that remain in these cases results in an unreliable measurement of x_C. The exponent found by the fit is $b = 0.24 \pm 0.03$. This is clearly in disagreement with the expected value of 1.0 that the simple operating tune error hypothesis predicts. It is much closer to the 1/3 value predicted by our first hypothesis of linear detuning, although there is a discrepancy that is unaccounted for at present.

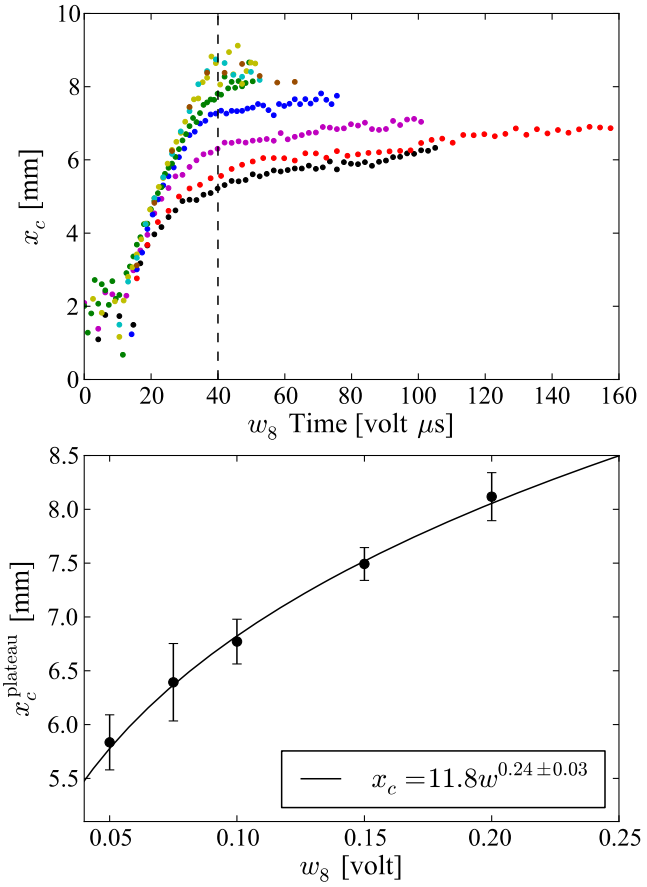

FIG. 11. The upper part of the figure shows the time evolution of the centroid amplitude calculated from ion loss data using Eq. (11). The measured size of the plasma distribution σ_x is 1.43 mm. The measured maximum centroid values are given by the mean of the centroid data from 40 V μs onwards, shown in the lower figure (black dots) together with the power law fit (solid black line).

Separately, we confirmed by numerical simulation that in the presence of nonlinearities it is possible to reproduce a similar plateau effect in ion loss observed in the experimental data, which is also shown in Fig. 5. In these simulations, sextupole and octupole terms were introduced at the level of about 0.5% of the quadrupole field.

From this experiment and simulation-based evidence, we can surmise that nonlinearities must play a role in the observed ion loss plateau behavior. In the future, it may be possible to investigate this effect in more detail if control over trap nonlinearities could be achieved.

B. Phase-dependent resonance-crossing effects

In Sec. III B, it was noted that the effects of resonance crossing are phase dependent in the situation where more than one integer resonance is crossed during an acceleration cycle. We made a conjecture that the amplitude of the coherent oscillation excited by the first integer resonance crossing could be subsequently enhanced or reduced depending on the phase of the coherent oscillation when the beam comes to the second integer resonance. To investigate this more thoroughly, the dependence on the relative initial phase was investigated experimentally for a fixed perturbation with varying crossing speed in Fig. 12. The abscissa represents the relative initial phase of the two sinusoidal dipole perturbation waves. The relative phase of zero degrees means that both perturbations start to grow from zero voltage at the same time. A period of oscillation is observed in the ion survival fraction, which depends on the relative phase between the first and second integer resonances, confirming the idea that observed ion loss fluctuates depending on the phase relation.

With a fixed crossing speed, the ion survival fraction depends on the dipole perturbation strength, as expected, but also the relative phase as seen in Fig. 13. In the best case, the effects of resonance crossing could be almost canceled even with a sizable dipole perturbation such as 0.2 V if the relative phase between the two resonances is arranged to be 130°.

However, in the case where a certain level of nonlinearity exists like in this LPT, the resultant incoherent tune spread gives rise to a smearing in the phase space. Note that the amplitude-dependent tune shift is small in a linear NS-FFAG like EMMA, where the major source of incoherent tune spread is the natural chromaticity and finite momentum spread, but the effects are analogous. The coherent dipole motion of the whole plasma is then diluted before

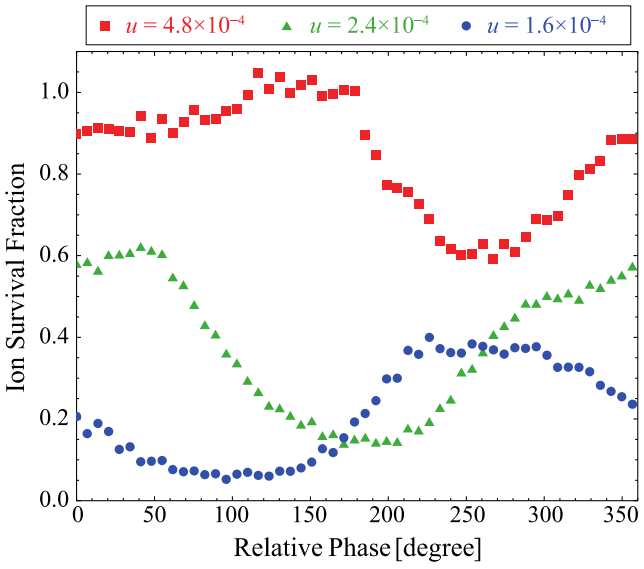

FIG. 12. Dependence of the ion survival fraction on the relative initial phase of the two sinusoidal dipole perturbations of a fixed strength. Three different speeds of resonance crossing are considered, namely, $u = 1.6 \times 10^{-4}$, $u = 2.4 \times 10^{-4}$, and $u = 4.8 \times 10^{-4}$. The range of tune sweeping is the same as in Fig. 10. The amplitudes of the eighth and ninth dipole harmonics are fixed at 0.2 V.

the second stop band is reached. Naturally, the smearing should be enhanced as the crossing speed is decreased (because it takes the operating point a longer period to move from one stop band to the next).

Experimental data in Fig. 10 support these expectations of double resonance crossing. Namely, the fine structure due to the relative phase almost disappears when the crossing speed is low. Therefore, the mechanism of enhancement or reduction of the centroid oscillation amplitude is relevant only when the smearing can be ignored on the time scale of the accelerator cycle. It is inadvisable for a machine to be operated in the parameter regime where sizable smearing occurs. The emittance would grow owing to smearing every time a beam traversed an integer resonance, and this is not tolerable in practical operation.

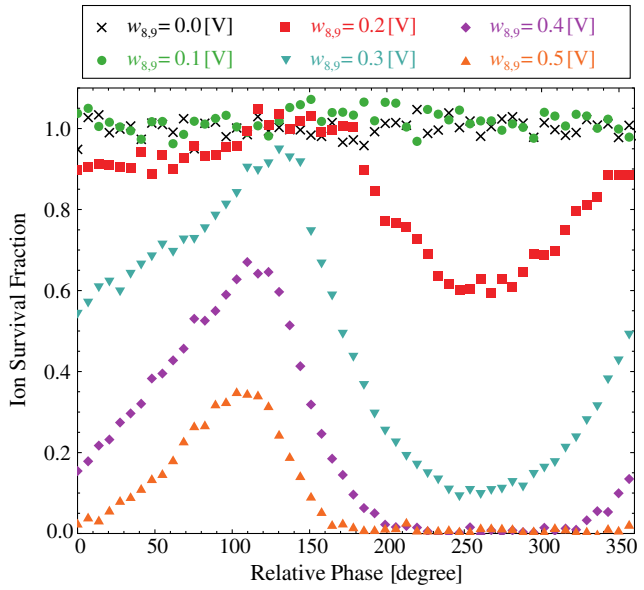

FIG. 13. Dependence of ion losses on the relative initial phase of the two sinusoidal dipole perturbations of various strengths (S-POD data). The crossing speed has been fixed at $u = 1.6\times10^{-4}$. The range of tune sweeping is the same as assumed in Fig. 10.

V. CONCLUDING REMARKS

In summary, we have first verified the theory of integer resonance crossing experimentally over a wide range of resonance strengths and crossing speeds. We have found that the mechanism of resonance crossing in terms of parameter dependence agrees with previous theoretical works. Additionally, we have found that the relative advance in the betatron phase between consecutive integer tunes needs to be considered when determining effects of amplitude growth from multiple resonance crossing. Nonlinear effects either due to the alignment of the trap in S-POD or due to chromaticity and momentum spread in a FFAG are unavoidable. This means there is an interplay between the relative phase effects and nonlinear effects which will result in a real emittance growth after integer crossing, not just the excitation of dipole oscillations. As such, when the decoherence time is short relative to the traversal time from one integer to another, cancellation from consecutive excitations cannot be expected. The interplay between these various effects needs to be considered in the design of proton and ion NS-FFAGs or other accelerators that routinely perform integer resonance crossing.

ACKNOWLEDGMENTS

This work is supported in part by a Grant-in-Aid for Scientific Research, Japan Society for the Promotion of Science. The work of one author (S. L. S.) was supported in part by the Royal Commission for the Exhibition of 1851 Brunel Fellowship.

APPENDIX A: SIMULATIONS OF AMPLITUDE GROWTH ON RESONANCE

Three independent approaches were used to cross-check numerical results in Sec. II D; these are (a) multiparticle simulations with the WARP code in 2D ignoring the space charge potential, as we are interested only in low-intensity effects in this case [37], (b) one-dimensional (1D) simulations based on Eq. (3), and (c) theoretical estimation from a rigid Gaussian model. Unlike the quadrupole and other nonlinear resonances, integer resonances do not give rise to a deformation of the initial ion distribution but simply cause a spatial shift of the whole plasma. Recalling this fact, in approach (c) we make a Gaussian plasma oscillate about the trap axis and calculate how much of the Gaussian tail

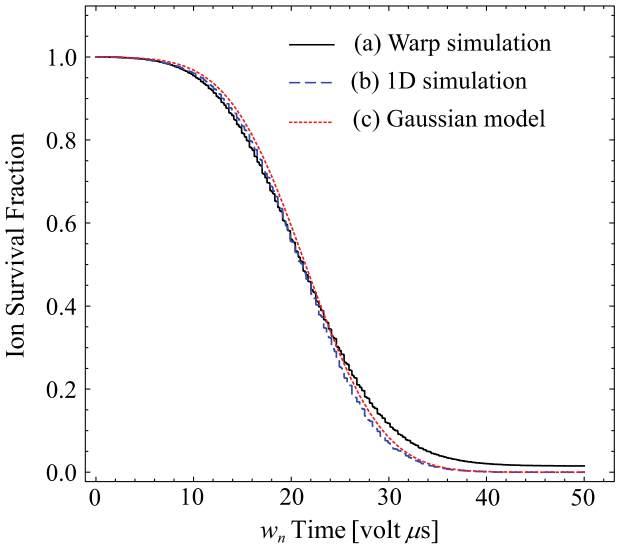

FIG. 14. Comparison of ion loss fractions evaluated from three independent numerical models.

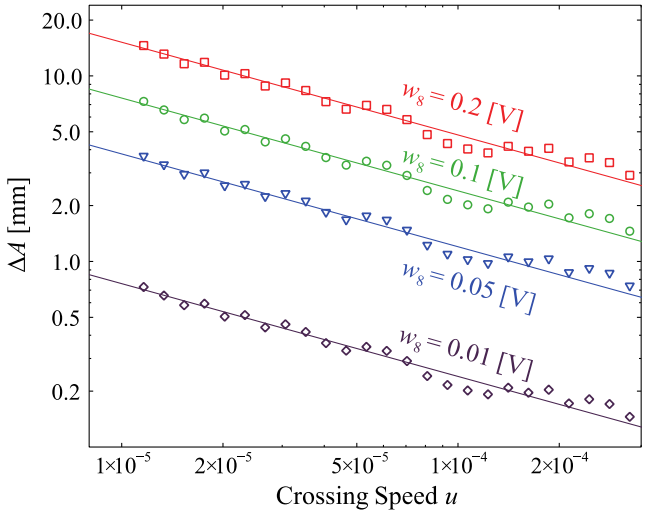

FIG. 15. Numerical results obtained from 2D WARP simulations without space-charge interactions and external nonlinear fields. The maximum transverse amplitude of an ion plasma after crossing the integer resonance stop band at $n = 8$ is plotted as a function of crossing speed u. The tune-variation range is chosen the same as in Fig. 8. The solid lines are given by the scaling law $\Delta A = g_8 w_8/\sqrt{u}$ with $g_8 = 0.30$.

crosses the circular boundary of 5 mm in radius. The time evolution of the centroid oscillation is determined by solving Eq. (1). Comparison between the three numerical models is shown in Fig. 14. We have confirmed that these approaches produce similar results as long as the trap has perfectly linear focusing.

APPENDIX B: SIMULATIONS OF SINGLE RESONANCE CROSSING

Figures 5 and 8 indicate that the numerical simulations can explain the experimental observations. This fact justifies the use of WARP or even a simpler 1D code for a quick estimate of the transverse amplitude of the plasma centroid after resonance crossing unless the nonlinear effect is too strong. The maximum centroid shifts ΔA_n numerically evaluated with various dipole perturbation strengths are plotted in Fig. 15 as a function of crossing speed u. The existence of the quadrupole electrodes is ignored in this simulation, so that we can maintain all initial particles even after the oscillation amplitude exceeds the LPT aperture size. A pure rf quadrupole focusing field is assumed to eliminate nonlinear effects. The fitting lines in Fig. 15 indicate that ΔA_8 scales as $\Delta A_8 = g_8 w_8/\sqrt{u}$, where the constant g_8 is close to 0.30. This is consistent with Eq. (8) derived without the smooth approximation [38] as well as the smooth-approximated formula in Refs. [41,42]. Under the smooth approximation, we have the same scaling formula as Eq. (8) with a different coefficient, namely,

$$\Delta A_n = g_n^{\mathrm{B}} \frac{w_n}{\sqrt{u}}, \tag{B1}$$

where $g_n^{\mathrm{B}} = (Pq\lambda^2/4\pi mc^2 r_0)/n$. Putting $n = 8$, we have $g_8^{\mathrm{B}} \approx 0.20$, for example. In Fig. 16, we have compared this coefficient g_n^{B} with the nonsmoothed coefficient g_n^{G} and with WARP simulation results. The enhanced disagreement for a higher n value is found in g_n^{B}. We have confirmed that the prediction from the nonsmooth formula results in better agreement with numerical simulation results over a wide range of n value.

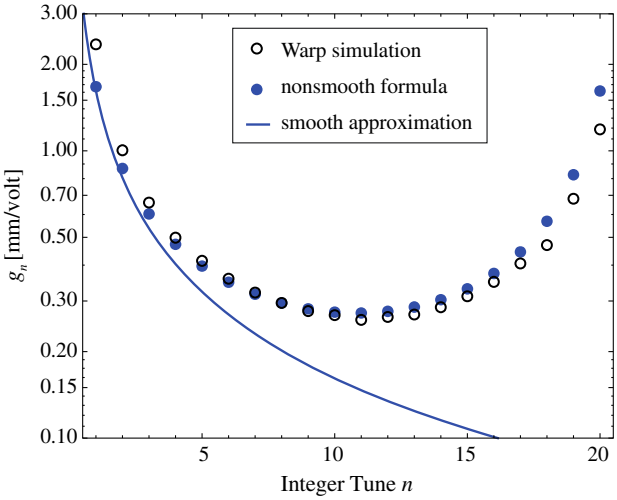

FIG. 16. Comparison of the coefficient g_n^G in the nonsmoothed scaling formula (8) and g_n^B in the smoothed scaling formula (B1). The values of g_n^G at different harmonic numbers n are plotted with black dots. The solid line comes from the definition of g_n^B in Eq. (B1). Open circles represent the corresponding WARP simulation results.

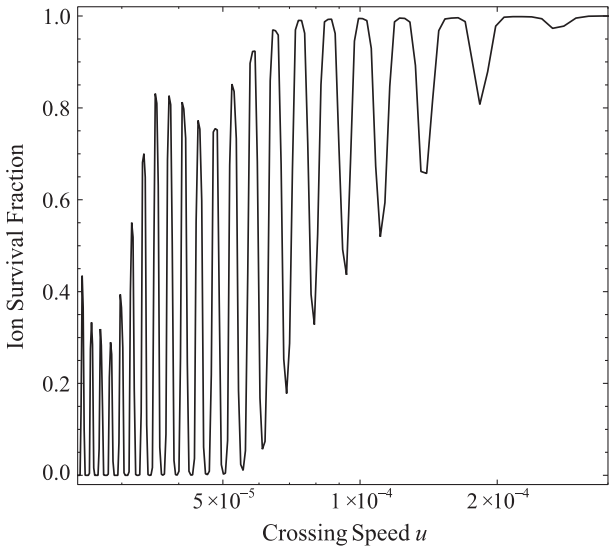

FIG. 17. WARP simulation results of double resonance crossing in the absence of external field nonlinearity and space charge. The relative phase between the eighth and ninth dipole harmonics has been fixed at 0° in this example.

APPENDIX C: PHASE DEPENDENCE SIMULATIONS

Numerical simulations based on a simple linear focusing model have shown strong oscillatory dependence of ion losses on the crossing speed as shown in Fig. 17. When the second kick is given at the optimal timing, the ion losses from the second resonance crossing can be suppressed almost completely. Such a favorable effect can, however, be expected only when the external nonlinearity is negligible, as stated in Sec. IV.

[1] F. Mills, in *Proceedings of the Fourth International Conference on Physics Potential and Development of* $\mu^+\mu^-$ *Colliders, Transparency Book, UCLA, 1997*, p. 693.

[2] C. Johnstone, in Ref. [1], p. 696.

[3] C. Johnstone, W. Wan, and A. Garren, in *Proceedings of the 18th Particle Accelerator Conference, New York, 1999* (IEEE, New York, 1999), p. 3068.

[4] The authors acknowledge that the possibility of violating the scaling law was first mentioned in the 1950s as discussed in L. W. Jones, AIP Conf. Proc. **237**, 1 (1991). However, the first design for a nonscaling FFAG was not published until the 1990s, hence the term "invention" as stated.

[5] E. Keil and A. M. Sessler, Nucl. Instrum. Methods Phys. Res., Sect. A **538**, 159 (2005).

[6] M. Apollonio *et al.* (ISS Accelerator Working Group), JINST **4**, P07001 (2009).

[7] K. R. Symon, D. W. Kerst, L. W. Jones, L. J. Laslett, and K. M. Terwillinger, Phys. Rev. **103**, 1837 (1956).

[8] M. Aiba *et al.*, in *Proceedings of the European Particle Accelerator Conference, Vienna, 2000* (EPS, Geneva, 2000), p. 581.

[9] M. Tanigaki *et al.*, in *Proceedings of the 10th European Particle Accelerator Conference, Edinburgh, Scotland, 2006* (EPS-AG, Edinburgh, Scotland, 2006), p. 2367.

[10] Y. Mori, Nucl. Instrum. Methods Phys. Res., Sect. A **562**, 591 (2006).

[11] E. Keil, A. M. Sessler, and D. Trbojevic, Phys. Rev. ST Accel. Beams **10**, 054701 (2007).

[12] K. J. Peach *et al.*, Phys. Rev. ST Accel. Beams **16**, 030101 (2013).

[13] R. Barlow, S. Tygier, and A. Toader, in *Proceedings of the International Particle Accelerator Conference, Kyoto, Japan* (ICR, Kyoto, 2010), p. 564.

[14] S. L. Sheehy, K. J. Peach, H. Witte, D. J. Kelliher, and S. Machida, Phys. Rev. ST Accel. Beams **13**, 040101 (2010).

[15] C. Johnstone, M. Berz, K. Makino, S. Koscielniak, and P. Snopok, Int. J. Mod. Phys. A **26**, 1690 (2011).

[16] R. Barlow *et al.*, Nucl. Instrum. Methods Phys. Res., Sect. A **624**, 1 (2010).

[17] S. Machida *et al.*, Nat. Phys. **8**, 243 (2012).

[18] S. Koscielniak and C. Johnstone, Nucl. Instrum. Methods Phys. Res., Sect. A **523**, 25 (2004).

[19] For example, integer resonances are routinely crossed in some cyclotrons.

[20] Work has been carried out to study slow resonance crossing using in-bucket synchrotron oscillations, but such experiments are limited in scope by the available parameter range. For details, see J. Garland *et al.*, in *Proceedings of the 3rd International Particle Accelerator Conference, New Orleans, LA, 2012* (IEEE, Piscataway, NJ, 2012), p. 412.

[21] S. L. Sheehy and D. J. Kelliher, Int. J. Mod. Phys. A **26**, 1842 (2011).

[22] D. Trbojevic, M. Blaskiewicz, and E. Forest, Int. J. Mod. Phys. A **26**, 1852 (2011).

[23] H. Okamoto and H. Tanaka, Nucl. Instrum. Methods Phys. Res., Sect. A **437**, 178 (1999).

[24] H. Okamoto, Y. Wada, and R. Takai, Nucl. Instrum. Methods Phys. Res., Sect. A **485**, 244 (2002).

[25] R. Takai, H. Enokizono, K. Ito, Y. Mizuno, K. Okabe, and H. Okamoto, Jpn. J. Appl. Phys. **45**, 5332 (2006).

[26] S. Ohtsubo, M. Fujioka, H. Higaki, K. Ito, H. Okamoto, H. Sugimoto, and S. M. Lund, Phys. Rev. ST Accel. Beams **13**, 044201 (2010).

[27] H. Takeuchi, K. Fukushima, K. Ito, M. Moriya, H. Okamoto, and H. Sugimoto, Phys. Rev. ST Accel. Beams **15**, 074201 (2012).

[28] H. Okamoto, M. Endo, K. Fukushima, H. Higaki, K. Ito, M. Moriya, S. Yamaguchi, and S. M. Lund, Nucl. Instrum. Methods Phys. Res., Sect. A **733**, 119 (2014).

[29] K. Fukushima, K. Ito, H. Okamoto, S. Yamaguchi, K. Moriya, H. Higaki, T. Okano, and S. M. Lund, Nucl. Instrum. Methods Phys. Res., Sect. A **733**, 18 (2014).

[30] LPT is very popular these days and applied for a variety of purposes other than beam physics. See, e.g., P. K. Gosh, *Ion Traps* (Oxford Science, Oxford, 1995), and references therein.

[31] There are three LPT-based S-POD systems operational at Hiroshima University. We refer to the apparatus in Fig. 1 as "S-POD III." Other S-PODs are used for different beam physics experiments. For more information, see Ref. [28].

[32] R. C. Davidson, H. Qin, and G. Shvets, Phys. Plasmas **7**, 1020 (2000).

[33] E. P. Gilson, R. C. Davidson, P. C. Efthimion, and R. Majeski, Phys. Rev. Lett. **92**, 155002 (2004).

[34] E. P. Gilson, M. Chung, R. C. Davidson, P. C. Efthimion, and R. Majeski, Phys. Rev. ST Accel. Beams **10**, 124201 (2007).

[35] E. P. Gilson, R. C. Davidson, P. C. Efthimion, R. Majeski, E. A. Startsev, H. Wang, S. Koppell, and M. Talley, Phys. Plasmas **20**, 055706 (2013).

[36] In fact, in EMMA there is in addition a large septum leakage field of 0.6×10^{-3} Tm. To emulate this strong local dipole kick in S-POD, we need a rather high dipole voltage [namely, V_D near 50 V according to Eq. (6)] that causes almost instant ion losses due to the limited aperture of the current LPT design.

[37] D. P. Grote, A. Friedman, G. D. Craig, I. Haber, and W. M. Sharp, Nucl. Instrum. Methods Phys. Res., Sect. A **464**, 563 (2001).

[38] G. Guignard, Intersecting Storage Rings Division Report No. CERN 77–10, 1977.

[39] S. Machida, Phys. Rev. ST Accel. Beams **11**, 094003 (2008).

[40] S. R. Mane and W. T. Weng, Nucl. Instrum. Methods Phys. Res., Sect. A **306**, 9 (1991).

[41] R. Baartman, in *Proceedings of the FFAG Workshop, Vancouver, B.C., Canada, 2004*.

[42] S. Koscielniak and R. Baartman, in *Proceedings of the 21st Particle Accelerator Conference, Knoxville, TN, 2005* (IEEE, Piscataway, NJ, 2005), p. 3206.